Specific loss power of magnetic nanoparticles: A machine learning approach

APL Materials

Specific loss power of magnetic nanoparticles: A machine learning approach

Cite as: APL Mater. **10**, 081108 (2022); https://doi.org/10.1063/5.0099498
Submitted: 17 May 2022 • Accepted: 20 July 2022 • Published Online: 18 August 2022

Marco Coïsson, Gabriele Barrera, Federica Celegato, et al.

Specific loss power of magnetic nanoparticles: A machine learning approach

Cite as: APL Mater. 10, 081108 (2022); doi: 10.1063/5.0099498
Submitted: 17 May 2022 • Accepted: 20 July 2022 •
Published Online: 18 August 2022

Marco Coïsson,[a] Gabriele Barrera, Federica Celegato, Paolo Allia, and Paola Tiberto

AFFILIATIONS

INRIM, Advanced Materials and Life Sciences Division, Strada delle Cacce 91, 10135 Torino (TO), Italy

[a]Author to whom correspondence should be addressed: m.coisson@inrim.it

ABSTRACT

A machine learning approach has been applied to the prediction of magnetic hysteresis properties (coercive field, magnetic remanence, and hysteresis loop area) of magnetic nanoparticles for hyperthermia applications. Trained on a dataset compiled from numerical simulations, a neural network and a random forest were used to predict power losses of nanoparticles as a function of their intrinsic properties (saturation, anisotropy, and size) and mutual magnetic interactions, as well as of application conditions (temperature, frequency, and applied field magnitude), for values of the parameters not represented in the database. The predictive ability of the studied machine learning approaches can provide a valuable tool toward the application of magnetic hyperthermia as a precision medicine therapy tailored to the patient's needs.

Cancer being one of the most important causes of death,[1] its fight is a challenge that involves many different disciplines. Besides medical, clinical, biological, and pharmaceutical research, physical sciences and engineering have provided important contributions in developing materials and techniques for both diagnostics and therapy.[2–4] More recently, machine learning has emerged as a tool that brings together multiple different disciplines by helping aggregate and analyze the data and results emerging from the respective research fields; as such, it offers a new paradigm for their interpretation and for extracting valuable information to the benefit of final users,[5–10] including medical doctors and clinicians and, eventually, patients. Machine learning exploits the ability of suitably conceived algorithms to delve into large datasets and identify hidden or obscure links among data, helping establishing correlations and possible cause–effect relationships that would have passed unnoticed.[11] As a consequence, machine learning is nowadays considered a new frontier in many scientific domains, including research related to the fight against cancer.[12–15]

In recent years, the possibility to exploit the properties of nanoparticles to offer a different approach for cancer treatment has been investigated under a multitude of approaches. Among them, magnetic nanoparticles have been identified as potentially relevant in precision medicine through magnetic hyperthermia,[16,17] a technique aimed at delivering heat to tumor cells by inducing power losses into the magnetic nanoparticles by means of an externally applied electromagnetic field and therefore by releasing heat into the surrounding tissues. The heat, selectively released in the cancerous tissues, directly destroys them, or weakens them to improve the effectiveness of chemotherapy or radiotherapy, or helps to release a suitable drug locally.

With this paper, we aim at showing how machine learning can be exploited to predict the power losses of magnetic nanoparticles with different magnetic properties in a multitude of application conditions (e.g., temperature, mutual magnetic interactions, applied magnetic field intensity, and frequency), starting from an available database. In perspective, this approach will offer a fast, reliable, and easy to use tool available to medical doctors and magnetic hyperthermia operators for precisely and effectively tailoring the therapy to their patients' needs. In its present form, it provides a novel and viable method to model the magnetic properties of nanoparticles from an initial dataset. To eventually bring this approach to end users (e.g., medical doctors in hospitals), the property dataset will need to be expanded with additional simulated and experimental data on magnetic nanoparticles as well as with relevant information concerning the environment where the nanoparticles are expected to operate (e.g., kind of tissue where they are injected and its thermal transport properties), obtained either experimentally or by numerical simulations. The usefulness of the predictions presented by the machine learning models will increase in the course of time with the completeness of the training dataset, which will require a large,

collaborative, and multidisciplinary effort to be built. Proving the viability of the approach, starting from the modeling of the magnetic nanoparticles properties, is the aim of this paper.

In a typical magnetic hyperthermia application, magnetic nanoparticles are either injected or carried into the cancerous tissue and then submitted to an alternating electromagnetic field of suitable intensity and frequency, submitted to biocompatibility constraints, with the aim to induce in the target tissue an increase of temperature capable of killing, or at least weakening, the tumor cells. In many cases of interest, it can be assumed that particles are basically immobilized in the target tissues so that the dynamic magnetization by effect of a high-frequency magnetic field arises from the rotation of the local magnetization vector, without involving effects produced by the physical rotation of the particle's crystallographic axes or by the displacement of particles in space. Many different parameters contribute in determining the end result; all need to be under the control of the operator; otherwise, either an insufficient or excessive amount of heat is released, which respectively turns out to be ineffective or dangerous. Among the involved parameters, the more relevant ones can be collected into three different groups, according to Fig. 1:

- **Application conditions:** the parameters that are under the control of the operator are placed in this group. The involved quantities are temperature T at which the nanoparticles power losses are exploited; the vertex field H_V, i.e., the maximum applied magnetic field (in absolute value), representing the field extrema between which the hysteresis loop is cycled and the power losses are exploited; and the frequency ν at which the applied field cycles.
- **Material:** the parameters that describe the intrinsic properties of nanoparticles are placed in this group. The involved quantities are saturation magnetization M_S, magnetic anisotropy K, nanoparticles diameter D, and magnetic interaction parameter Int [defined as $Int = \frac{D}{d}$, where D is the nanoparticle diameter and d is their (average) center-to-center distance]. Therefore, when the nanoparticles are infinitely far apart, $Int = 0$, and when the nanoparticles are so close to each other that they touch (their distance is equal to their diameter), then $Int = 1$. A more thorough discussion on the role and meaning of the interaction parameter is available in the supplementary material (simulated data).
- **Loop shape:** the parameters that describe the hysteresis loop shape are placed in this group. The involved quantities are coercive field H_C, magnetic remanence M_R, and hysteresis loop area *area* (intimately linked to the specific loss power, SLP, and interaction parameter[18]).

It is important to remark that these parameters may not be uniquely defined in real magnetic nanoparticles ensembles, where most notably size and anisotropy distributions can be significant, especially when large amounts of nanoparticles are required,[19] that are prepared in different batches with different properties. For such applications, techniques (e.g., Ref. 20) capable to prepare homogeneous, large batches of nanoparticles might be of relevance to help in uniquely defining the above parameters better. Moreover, they may not be the only relevant ones. For example, in a real magnetic hyperthermia application, the kind of tissue that is the target of the therapy will play a role, as its thermal transport properties will have to be taken into account to properly quantify the amount of particles to be injected into the tumor. However, in this paper, we will focus only on the parameters shown in Fig. 1. All of them are subject to several non-linear relationships that are schematically represented by the color codes and the puzzle-like shapes in Fig. 1. For example, the temperature (red box) directly affects M_S and K values; however, these quantities are not entirely defined by T; therefore, in Fig. 1, they are represented as more complex shapes, with orange boxes, the orange color identifying a non-linear relationship that is hidden in the model used to describe these quantities. In turn, M_S, together with the interaction parameter, affects the loop shape that

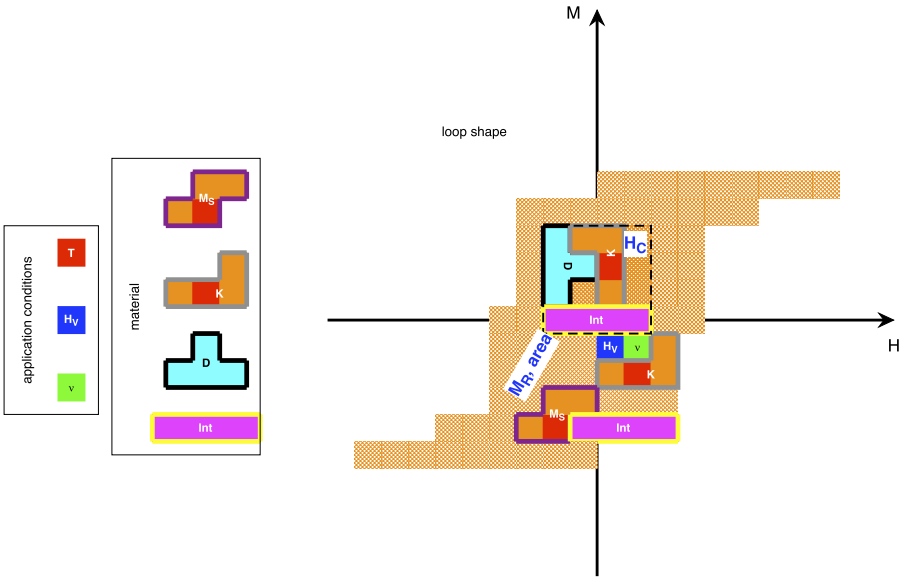

FIG. 1. Schematic representation of the relationships among the different quantities taken into account in the two-well model.

is again composed of the M_S block but also of other orange boxes, representing the complex model gluing all together. However, the interaction parameter plays with K and D as well, directly affecting the coercive field H_C (represented as a complex block with dashed contour in Fig. 1), which, in turn, plays a role in determining the whole loop shape. Similarly, H_V and v, together with the magnetic anisotropy, also affect the final loop shape. All these relationships are often highly non-linear. Under specific constraints, some of these non-linear relationships can be analytically modeled, such as the dependence of the magnetic anisotropy or magnetic saturation on temperature,[21] the dependence of coercivity on particles size in the static condition for uniaxial Stoner–Wohlfarth nanoparticles,[21] and the dependence of the coercivity on the magnetic interactions of dipolar origin among the nanoparticles.[22] However, all these models require strong approximations, are sometimes incompatible with each other, and cannot take into account the whole complexity of a real system. As a consequence, an analytical representation of the non-linear relationships shown in Fig. 1 is not available. To overcome this limitation, numerical models are often developed, which try to take into account as many parameters as possible, at the expense of their complexity or of computation time.

Among these models, the two-well one[23,24] has been exploited to generate a large number of magnetic hysteresis loops of nanoparticles in different measurement conditions and for different material property values. In total, ~4000 (precisely: 3963) simulations have been carried on, and their data (the ten quantities listed in Fig. 1) are collected. The supplementary material (simulated data) provides a few examples of the relationships among selected quantities appearing in the two-well model, drawing from the whole set of simulated data. The orange boxes of Fig. 1, then, can be thought of as being "filled" with the two-well model, which sticks together all the parameters, in an appropriate way, to reproduce the final loop shape for a given set of application conditions and material parameters.

While large, the simulated dataset cannot cover any possible scenario where the prediction of the hysteresis loop details of an ensemble of nanoparticles with given properties and in a given experimental condition would be important. Exploiting the two-well model to generate the simulations in the desired conditions requires both a specific expertise on the model and on the required numerical tools and sufficient computation time. In fact, the calculation of an hysteresis loop of magnetic systems, especially in conditions far from magnetic saturation, is a task that cannot be significantly parallelized, since the magnetization processes are characterized by a memory[25] that is often *non-persistent* (and therefore depends on the rate at which the applied magnetic field is varied) and *non-local* (and therefore not only the present state but the whole past history of the magnetic material need to be known to calculate its future states). As a consequence, except for very simple models and systems, the accurate calculation of the magnetic configuration or of the hysteresis loop of a magnetic system, under given conditions, is computationally heavy. However, in a perspective future application, a magnetic hyperthermia clinical operator (e.g., a medical doctor) would need reliable and fast tools, letting them concentrate on the specifics of the treatment to be administered to the patient; these conventional numerical models, requiring the setup of proper simulation parameters and a long waiting time (maybe hours or days), are not adequate for this purpose. On the contrary, innovative machine learning approaches seem particularly apt at overcoming these severe obstacles.

Machine learning systems, fed with appropriate input quantities, have already been proven as valuable tools to model and predict relevant magnetic properties of materials.[26–29] We aim at demonstrating that a machine learning system can offer, in almost real time, the requested predictions in terms of hysteresis loops properties (coercivity, remanence, and area) as a function of the parameters that must be optimized (e.g., particles size, their concentration in the medium, and maximum applicable magnetic field) in a magnetic hyperthermia application. In perspective, a software with a simple user interface, on a commodity personal computer (PC) or directly on the computer supporting the magnetic hyperthermia clinical equipment and having access to a suitable set of simulated (or experimental) data, could provide in a few seconds all the information the medical doctor would need to optimize the treatment for the patient, without needing to delve into the details of the two-well (or any other physical) model or of the numerical tools required to solve its equations.

Therefore, we decided to use the set of 3963 simulations obtained with the two-well model to train and test two different machine learning systems, both having the quantities reported in Fig. 1 "application conditions" and "material" boxes as inputs and those in the "loop shape" box as outputs. Once more, the orange boxes in Fig. 1 can now be thought of as "filled" with the machine learning models that provide the necessary non-linear relationships among all the relevant quantities to produce the desired outputs (M_R, H_C, and *area*). The two systems are a neural network and a random forest, whose details are briefly reported in the supplementary material (machine mearning). Unless otherwise declared, the neural network and the random forest have been randomly initialized each time and trained with a random subset of the whole simulated dataset, made of 90% of it [see the supplementary material (machine learning) for more details]. Then, the two machine learning systems have been tested on the remaining 10% of the whole dataset. Each result has been repeated 30 times with a different (random) initialization of the machine learning system and training-testing splitting of the whole dataset. Scores and predicted values are then averaged and their standard deviation is calculated to give the final results and their respective error bars, as reported in the following.

Ten representative cases, whose parameters are reported in the supplementary material (machine learning), have been chosen for looking into the details of the predictions obtained by machine learning and comparing them with the expected values obtained through the two-well model simulations. Figure 2 reports the results. For both the neural network and the random forest, the predicted values for the output quantities (H_C, M_R and *area*) are plotted as a function of their respective expected (true) values. Ideally, the data should be on the bisector. Overall, this is the case, considering the error bar (calculated as described above) for each point.

Perusal of Fig. 2 reveals that the neural network provides more scattered output values (their error bars are larger) than the random forest, while the score as calculated by the regressor (and averaged over the 30 repetitions) on the testing set is significantly lower. Both machine learning systems provide comparable results in terms of deviations relative to σ (σ being the standard deviation), as shown in

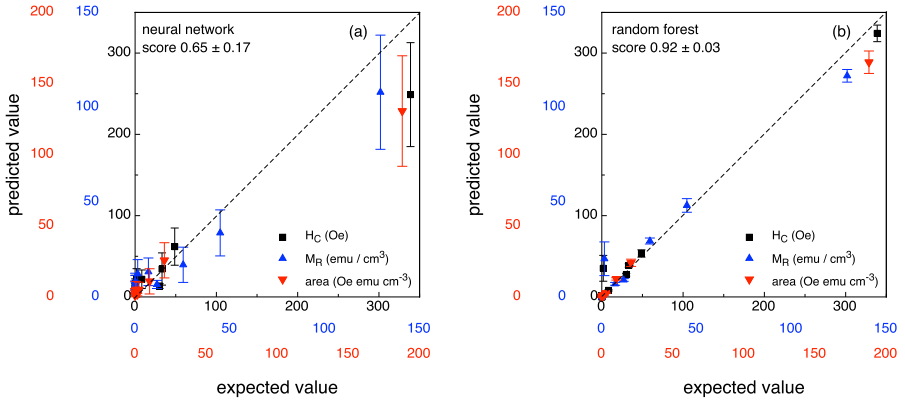

FIG. 2. (a) Neural network and (b) random forest predictions for H_C, M_R, and *area* values as a function of the expected (true) values. The dashed lines are a guide to the eye. Axes labels are in the same color as the data points. The scores are obtained by averaging those calculated by the respective regressors for each repetition.

Fig. 3, where in the abscissa the relative difference between the predicted value p_v (by the machine learning system) and the expected value e_v is reported for H_C, M_R, and loop *area*. In fact, the vast majority of the predicted data are within 3σ of the expected value, as indicated by the dashed line in Fig. 3(a). However, the random forest has much lower σ values, indicating that it is more precise in its predictions and its computing time (~1 min on our computer) is on average 300 times shorter than for the neural network. As a consequence, the random forest system appears to be both quicker and more precise and will be the only one used in the following.

The power of the machine learning approach can now be fully exploited to generate results for input parameter values that were not previously simulated. The medical doctor of our previous examples could therefore be interested in optimizing the treatment for the patient. In the actual treatment conditions, the tissues receiving the hyperthermia treatment will be at 42 °C (315 K, a temperature not simulated in the training dataset). The nanoparticles will be excited by an alternating field at a frequency, for example, of 100 kHz, but biomedical constraints would impose a maximum field amplitude H_V = 150 Oe (a value not simulated in the training dataset). The optimum nanoparticles size (without interactions) can then be obtained by calculating the predicted area as a function of the nanoparticles diameter, as shown in Fig. 4(a). The medical doctor can then choose the nanoparticles, among those that are available in the hospital, with an average diameter of ≈12.5 nm. However, even for these nanoparticle sizes, the applied field might not have the value offering best performance. Figure 4(b), obtained by extending the simulations over a much finer field resolution through the random forest interpolation, then shows that if the medical doctor could increase H_V to ~250 Oe, then the loop area (and therefore the SLP, and the heat released by the particles to the patient tissues) would dramatically increase, thus obtaining a significantly improved performance. Further increasing H_V, however, would not induce any additional improvements because at that threshold, the major hysteresis loop has probably already been exploited; thus, a further increase of the vertex field does not result in an increased loop area. It is worth noting that Fig. 4(b) does not contain only interpolation but also extrapolation, as values of H_V above 500 Oe are not part of the training set of the machine learning model.

If the medical doctor cannot increase the applied field intensity for safety reasons, the performance of the nanoparticles can still be improved by playing with their concentration [or the interaction parameter, see Fig. 4(c)]: increasing the *Int* parameter from zero to ≈0.6 improves the SLP value (the loop area), therefore leading to an optimized performance of the treatment. This non-monotonous behavior of the power losses as a function of the interactions among the nanoparticles is a non-trivial effect,[30–37] which has been discussed in the literature sometimes with contrasting conclusions.

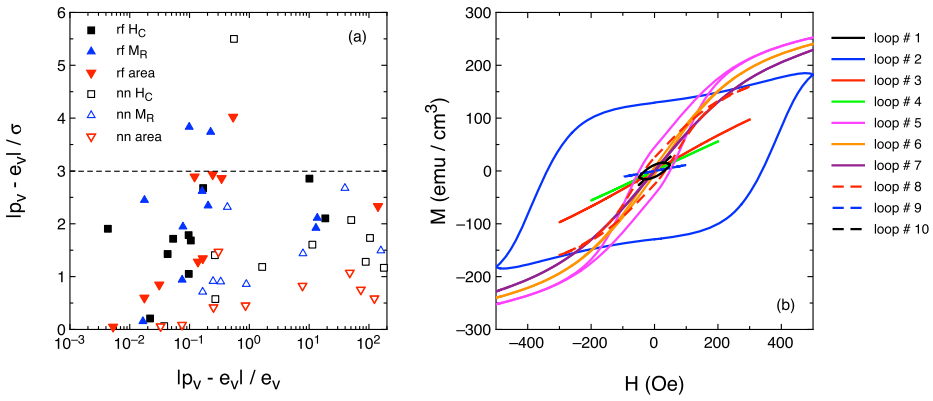

FIG. 3. (a) Deviation of the predicted value p_v from the expected one e_v, divided by the standard deviation, for the ten elements of Fig. 2. Full symbols refer to the random forest system, and open symbols refer to the neural network system. The dashed line marks the 3σ threshold. (b) Respective hysteresis loops. The loops data are reported in the supplementary material (machine learning).

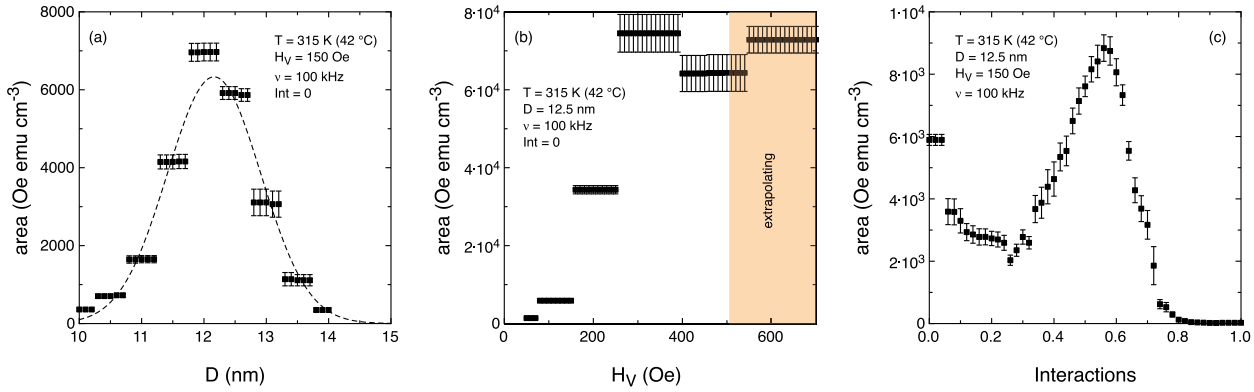

FIG. 4. (a) Loop area as a function of nanoparticles diameter for the reported measurement conditions. The dashed line is a guide to the eye. (b) Loop area as a function of the vertex field. (c) Loop area as a function of the interaction parameter.

While a systematic numerical study of this effect could be difficult and time consuming, machine learning approaches could help exploring how interactions among magnetic nanoparticles affect their specific loss power in a more effective way. Moreover, the predictions reported in Fig. 4 are accurate and physically sound, as discussed in the supplementary material (machine learning) by comparing them against numerically simulated[24,38] and experimental data.[39,40]

Each of the optimization steps reported above as examples relies on data simulated once-for-all and exploits machine learning approaches to interpolate the outputs in conditions not represented in the original training dataset; moreover, they produce results almost in real time (the random forest is trained, tested, and used to obtain the predictions each time for 30 repetitions, in ~1 min in total on a commodity laptop) and could be triggered with a user interface hiding the complexity of the details, suitable for the in-field application. By contrast, the qualitatively similar results discussed in the supplementary material (machine learning) obtained with the two-well model require extremely longer computation times (days).

The revolution of precision medicine, tailoring treatments, and therapies to the specific needs and conditions of the patient cannot be fulfilled without the multidisciplinary contributions of different sciences and specialties. In the case of magnetic hyperthermia treatments, it is necessary that both the application conditions and the chosen nanoparticles are adapted to the tumor properties and position, to the patient health in general, to the concurrent therapies (e.g., chemotherapy, radiotherapy), etc. It is therefore required to have large datasets, either compiled experimentally or numerically, that provide as much information as possible but also innovative, powerful, and efficient methods that can process the ever growing input data giving, in almost real time, the necessary information to the magnetic hyperthermia operator or medical doctor. Magnetic hyperthermia, however, is not the only biomedical application of magnetic nanoparticles, with bioregenerative substrates and imaging techniques based on contrast agents made of magnetic nanoparticles being important examples. In addition, in these cases, similar approaches could be extremely useful to help selecting the proper materials and operating conditions in order to optimize the diagnostic or therapeutic effect of the magnetic nanoparticles. In this paper, we have shown that machine learning approaches, even on a relatively small dataset limited to simulated nanoparticles properties, can produce valuable outputs (e.g., hysteresis loop area) for a variety of application conditions and materials parameters using a dataset obtained with numerical simulations on a two-well model system. Future extended datasets and models could build on top of this approach by collecting both physical and clinical data from simulations and experiments and would eventually be extended to additional quantities and parameters relevant to the biological tissues and the patients' health conditions. In perspective, the aim is to build an improving-over-time knowledge base that will make machine learning systems more accurate in their predictions. The approach presented in this paper can therefore pave the way toward a breakthrough in the application of magnetic hyperthermia for cancer treatment.

See the supplementary material for details on the simulated dataset and how the different input quantities are represented in it (simulated data) and for details on the neural network and random forest models, for details on the testing dataset, and for a validation of the predictions with both simulated and experimental data available in the literature (machine learning).

AUTHOR DECLARATIONS

Conflict of Interest

The authors have no conflicts to disclose.

Author Contributions

Marco Coïsson: Conceptualization (lead); Formal analysis (lead); Investigation (lead); Methodology (lead); Software (lead); Validation (lead); Visualization (lead); Writing – original draft (lead); Writing – review & editing (lead). **Gabriele Barrera**: Conceptualization

(equal); Data curation (equal); Validation (equal); Writing – review & editing (equal). **Federica Celegato**: Writing – review & editing (supporting). **Paolo Allia**: Conceptualization (equal); Data curation (equal); Validation (equal); Writing – review & editing (equal). **Paola Tiberto**: Writing – review & editing (supporting).

DATA AVAILABILITY

The data that support the findings of this study are available from the corresponding author upon reasonable request.

REFERENCES

[1] H. Sung, J. Ferlay, R. L. Siegel, M. Laversanne, I. Soerjomataram, A. Jemal, and F. Bray, "Global cancer statistics 2020: GLOBOCAN estimates of incidence and mortality worldwide for 36 cancers in 185 countries," CA Cancer J. Clin. **71**, 209–249 (2021).

[2] S. F. Keevil, "Physics and medicine: A historical perspective," Lancet **379**, 1517–1524 (2012).

[3] H. Laufman, "Are engineers unsung heroes of medical progress?: The historic bond between physics, engineering, and medicine," Biomed. Instrum. Technol. **36**, 325–334 (2002).

[4] C. Fiorino, R. Jeraj, C. H. Clark, C. Garibaldi, D. Georg, L. Muren, W. van Elmpt, T. Bortfeld, and N. Jornet, "Grand challenges for medical physics in radiation oncology," Radiother. Oncol. **153**, 7–14 (2020).

[5] P. P. Shinde and S. Shah, "A review of machine learning and deep learning applications," *2018 Fourth International Conference on Computing Communication Control and Automation (ICCUBEA)* (IEEE, 2018).

[6] Y. Lei, B. Yang, X. Jiang, F. Jia, N. Li, and A. K. Nandi, "Applications of machine learning to machine fault diagnosis: A review and roadmap," Mech. Syst. Signal Process. **138**, 106587 (2020).

[7] J. J. Valletta, C. Torney, M. Kings, A. Thornton, and J. Madden, "Applications of machine learning in animal behaviour studies," Anim. Behav. **124**, 203–220 (2017).

[8] J. Vamathevan, D. Clark, P. Czodrowski, I. Dunham, E. Ferran, G. Lee, B. Li, A. Madabhushi, P. Shah, M. Spitzer, and S. Zhao, "Applications of machine learning in drug discovery and development," Nat. Rev. Drug Discovery **18**, 463–477 (2019).

[9] J. Hegde and B. Rokseth, "Applications of machine learning methods for engineering risk assessment–A review," Saf. Sci. **122**, 104492 (2020).

[10] J. Schmidt, M. R. G. Marques, S. Botti, and M. A. L. Marques, "Recent advances and applications of machine learning in solid-state materials science," npj Comput. Mater. **5**, 83 (2019).

[11] S. Pouyanfar, S. Sadiq, Y. Yan, H. Tian, Y. Tao, M. P. Reyes, M.-L. Shyu, S.-C. Chen, and S. S. Iyengar, "A survey on deep learning: Algorithms, techniques, and applications," ACM Comput. Surv. **51**, 92 (2019).

[12] C. J. Tsai, N. Riaz, and S. L. Gomez, "Big data in cancer research: Real-world resources for precision oncology to improve cancer care delivery," Semin. Radiat. Oncol. **29**, 306–310 (2019).

[13] Z. Dlamini, F. Z. Francies, R. Hull, and R. Marima, "Artificial intelligence (AI) and big data in cancer and precision oncology," Comput. Struct. Biotechnol. J. **18**, 2300–2311 (2020).

[14] J. Ko, N. Bhagwat, S. S. Yee, N. Ortiz, A. Sahmoud, T. Black, N. M. Aiello, L. McKenzie, M. O'Hara, C. Redlinger, J. Romeo, E. L. Carpenter, B. Z. Stanger, and D. Issadore, "Combining machine learning and nanofluidic technology to diagnose pancreatic cancer using exosomes," ACS Nano **11**(11), 11182–11193 (2017).

[15] Z. Gao, Y. Song, T. Y. Hsiao, J. He, C. Wang, J. Shen, A. MacLachlan, S. Dai, B. H. Singer, K. Kurabayashi, and P. Chen, "Machine-learning-assisted microfluidic nanoplasmonic digital immunoassay for cytokine storm profiling in COVID-19 patients," ACS Nano **15**(11), 18023–18036 (2021).

[16] E. A. Périgo, G. Hemery, O. Sandre, D. Ortega, E. Garaio, F. Plazaola, and F. J. Teran, "Fundamentals and advances in magnetic hyperthermia," Appl. Phys. Rev. **2**, 041302 (2015).

[17] A. B. Salunkhe, V. M. Khot, and S. H. Pawar, "Magnetic hyperthermia with magnetic nanoparticles: A status review," Curr. Top. Med. Chem. **14**, 572–594 (2014).

[18] M. Coïsson, G. Barrera, F. Celegato, L. Martino, S. N. Kane, S. Raghuvanshi, F. Vinai, and P. Tiberto, "Hysteresis losses and specific absorption rate measurements in magnetic nanoparticles for hyperthermia applications," Biochim. Biophys. Acta **1861**, 1545–1558 (2017).

[19] J. H. Grossman and S. E. McNeil, "Nanotechnology in cancer medicine," Phys. Today **65**(8), 38 (2012).

[20] G. V. Kurlyandskaya, S. M. Bhagat, A. P. Safronov, I. V. Beketov, and A. Larrañaga, "Spherical magnetic nanoparticles fabricated by electric explosion of wire," AIP Adv. **1**, 042122 (2011).

[21] B. D. Cullity and C. D. Graham, *Introduction to Magnetic Materials* (Wiley, 2008), ISBN: 9780471477419, Online ISBN: 9780470386323.

[22] P. Allia, M. Coïsson, M. Knobel, P. Tiberto, and F. Vinai, "Magnetic hysteresis based on dipolar interactions in granular magnetic systems," Phys. Rev. B **60**(17), 12207–12218 (1999).

[23] G. Barrera, P. Allia, and P. Tiberto, "Temperature-dependent heating efficiency of magnetic nanoparticles for applications in precision nanomedicine," Nanoscale **12**, 6360 (2020).

[24] G. Barrera, P. Allia, and P. Tiberto, "Dipolar interactions among magnetite nanoparticles for magnetic hyperthermia: A rate-equation approach," Nanoscale **13**, 4103 (2021).

[25] G. Bertotti, *Hysteresis in Magnetism* (Academic Press, San Diego, 1998), Chap. 2, ISBN: 0-12-093270-9.

[26] E. Y. Vedmedenko, R. K. Kawakami, D. D. Sheka, P. Gambardella, A. Kirilyuk, A. Hirohata, C. Binek, O. Chubykalo-Fesenko, S. Sanvito, B. J. Kirby, J. Grollier, K. Everschor-Sitte, T. Kampfrath, C.-Y. You, and A. Berger, "The 2020 magnetism roadmap," J. Phys. D: Appl. Phys. **53**, 453001 (2020).

[27] J. Nelson and S. Sanvito, "Predicting the Curie temperature of ferromagnets using machine learning," Phys. Rev. Mater. **3**, 104405 (2019).

[28] E. A. Périgo and R. N. d. Faria, "Artificial intelligence—Engineering magnetic materials: Current status and a brief perspective," Magnetochemistry **7**, 84 (2021).

[29] G. Katsikas, C. Sarafidis, and J. Kioseoglou, "Machine learning in magnetic materials," Phys. Status Solidi B **258**, 2000600 (2021).

[30] D. F. Coral, P. Mendoza Zélis, M. Marciello, M. d. P. Morales, A. Craievich, F. H. Sánchez, and M. B. Fernández van Raap, "Effect of nanoclustering and dipolar interactions in heat generation for magnetic hyperthermia," Langmuir **32**, 1201–1213 (2016).

[31] B. Mehdaoui, R. P. Tan, A. Meffre, J. Carrey, S. Lachaize, B. Chaudret, and M. Respaud, Phys. Rev. B **87**, 174419 (2013).

[32] G. T. Landi, "Role of dipolar interaction in magnetic hyperthermia," Phys. Rev. B **89**, 014403 (2014).

[33] C. Blanco-Andujar, D. Ortega, P. Southern, Q. A. Pankhurst, and N. T. K. Thanh, "High performance multi-core iron oxide nanoparticles for magnetic hyperthermia: Microwave synthesis, and the role of core-to-core interactions," Nanoscale **7**, 1768–1775 (2015).

[34] M. E. Sadat, R. Patel, J. Sookoor, S. L. Bud'ko, R. C. Ewing, J. Zhang, H. Xu, Y. Wang, G. M. Pauletti, D. B. Mast, and D. Shi, "Effect of spatial confinement on magnetic hyperthermia via dipolar interactions in Fe_3O_4 nanoparticles for biomedical applications," Mater. Sci. Eng., C **42**, 52–63 (2014).

[35] D. P. Valdés, E. Lima, Jr., R. D. Zysler, G. F. Goya, and E. De Biasi, "Role of anisotropy, frequency, and interactions in magnetic hyperthermia applications: Noninteracting nanoparticles and linear chain arrangements," Phys. Rev. Appl. **15**, 044005 (2021).

[36] L. C. Branquinho, M. S. Carrião, A. S. Costa, N. Zufelato, M. H. Sousa, R. Miotto, R. Ivkov, and A. F. Bakuzis, "Effect of magnetic dipolar interactions on nanoparticle heating efficiency: Implications for cancer hyperthermia," Sci. Rep. **3**, 2887 (2013).

[37]C. Haase and U. Nowak, "Role of dipole-dipole interactions for hyperthermia heating of magnetic nanoparticle ensembles," Phys. Rev. B **85**, 045435 (2012).
[38]P. Allia, G. Barrera, and P. Tiberto, "Nonharmonic driving fields for enhancement of nanoparticle heating efficiency in magnetic hyperthermia," Phys. Rev. Appl. **12**, 034041 (2019).
[39]G. Barrera, M. Coïsson, F. Celegato, L. Martino, P. Tiwari, R. Verma, S. N. Kane, F. Mazaleyrat, and P. TIberto, "Specific loss power of Co/Li/Zn-mixed ferrite powders for magnetic hyperthermia," Sensors **20**, 2151 (2020).
[40]M. Coïsson, G. Barrera, C. Appino, F. Celegato, L. Martino, A. P. Safronov, G. V. Kurlyandskaya, and P. Tiberto, "Specific loss power measurements by calorimetric and thermal methods on γ-Fe_2O_3 nanoparticles for magnetic hyperthermia," J. Magn. Magn. Mater. **473**, 403–409 (2019).